Journal of Manufacturing Processes 83 (2022) 488–501

Contents lists available at ScienceDirect

Journal of Manufacturing Processes

journal homepage: www.elsevier.com/locate/manpro

Surface morphology and microstructure of the hole sidewall during drilling of Polyether-Ether-Ketone(PEEK) via single-pulse laser

Yanmei Zhang [a,c], Shaoxia Li [a,c], Yucui Yu [a,c], Chongxin Tian [a,c], Zhiyong Li [a,c], Yue Zhang [a,c], Xiuli He [a,c,*], Gang Yu [a,b,c,*]

[a] Institute of Mechanics, Chinese Academy of Sciences, Beijing 100190, China
[b] Center of Materials Science and Optoelectronics Engineering, University of Chinese Academy of Sciences, Beijing 100049, China
[c] School of Engineering Science, University of Chinese Academy of Sciences, Beijing 100049, China

ARTICLE INFO

Keywords:
Single-pulse laser drilling
Polyether-ether-ketone (PEEK)
Surface morphology
Microstructure
Material-removal mechanism

ABSTRACT

Polyether-ether-ketone (PEEK), as one kind of thermoplastic polymers, exhibits a great deal of remarkable properties and plays an important role in aerospace, electronics, automotive and medicine. An investigation of single-pulse laser drilling on Polyether-ether-ketone (PEEK) was reported to show the influence of irradiation energy on the hole sidewall. In-situ evolution of drilling process was observed by the high-speed camera. The surface morphology and microstructural characteristics of the hole sidewall were evaluated by different characterization techniques. The hole sidewall was divided into three parts: expanded zone at the entrance, linear zone in the middle, and U-shaped zone at the bottom. It was found that the quality of inner sidewall could be obviously improved under high single-pulse energy (>1 J), in terms of the surface morphology with small heat-affected zone (HAZ) thickness and surface roughness, as well as the least adhesion. Besides, chemical and structural characteristics of the hole sidewall changed a lot under high energy. The C content of three parts increased as the energy increased. The crystallinity of the hole sidewall decreased from 35 % to 25 % after laser-energy irradiation, but there was little change under different single-pulse energy. New diffraction peaks appeared in X-ray diffraction images and the intensity of the relative peaks in Raman spectra decreased when the energy was over 1 J. It was proven that some chemical bonds (phenyl ring (1597 cm^{-1}) and C–O–C (1148 cm^{-1})) would break under high energy, contributing to mass removal of the keyhole. Moreover, the HAZ thickness of the hole sidewall was calculated based on a viscous flow model, which showed a good consistency with experimental results. These results reveal material-removal mechanism accompanying the appearance of direct decomposition of the material and breaking of chemical bonds under high energy. It can provide references for understanding mechanisms of HAZ formation and material-removal and improving surface quality for laser drilling of polymers.

1. Introduction

New high-performance polymers are produced to meet ever increasing demand for materials in the industrial applications. Polyether-ether-ketone (PEEK), as one kind of thermoplastic polymer, exhibits a great deal of remarkable properties and plays an important role in aerospace, electronics, automotive, medicine and particularly in the biomedical application [1,2]. It has been gradually applied in the cranial repair instead of titanium alloy due to its superior biocompatibility [3,4]. A large number of high-precision micro-holes with large hole depth (>1 mm) and high aspect-ratio need to be processed on a PEEK matrix as the repair material. The distribution of many micro-holes is favorable for the extension of cell pseudopodia and the integration of bone-implant [5].

It is important to develop an efficient machining method for micro-holes on PEEK with excellent quality. Single-pulse laser drilling is a suitable method when many holes need to be drilled, owing to its characteristics of the high-efficiency, non-contact, and no-restriction of materials [6]. Compared with nanosecond, picosecond or femtosecond pulsed laser, the microsecond or millisecond pulsed laser has a higher material-removal rate [7]. However, the heat-affected zone (HAZ) is inevitable for the microsecond or millisecond laser drilling. Fusion and thermal decomposition occur during the process of laser ablation. The molten or vaporized material is not completely expelled and will be

* Corresponding authors at: Institute of Mechanics, Chinese Academy of Sciences, Beijing 100190, China.
E-mail addresses: xlhe@imech.ac.cn (X. He), gyu@imech.ac.cn (G. Yu).

https://doi.org/10.1016/j.jmapro.2022.09.023
Received 29 July 2022; Received in revised form 14 September 2022; Accepted 16 September 2022
Available online 22 September 2022

accumulated on the hole sidewalls as the HAZ. In addition, the chemical composition and crystallinity may change under the laser irradiation. Therefore, surface morphology and microstructure characteristics of the hole sidewall play an important role in assessing the drilling quality and analyzing the material-removal mechanism.

Some studies have been carried out to investigate the influence of laser processing parameters on the surface morphology and microstructure of polymers. The influence of CO_2 laser radiation on the surface properties of PEEK was studied [8]. It was found that the surface roughness increased with increasing laser intensity but the change of surface chemistry was nearly negligible. The effects of laser energy on the ablation depth and surface quality were examined for the polyimide (PI) film ablation using 355 nm DPSS Nd: YVO_4 laser [9]. Experimental results showed that the high-quality surface was achieved with no deformation or burr when the laser energy was lower than the threshold energy. For laser cutting of plastics (polyester resin), it could be concluded that the kerf morphology was obtained with good quality and high productivity under high-power laser systems and high-speed feed rates [10]. The influence of the processing parameters on the interaction phenomena and the HAZ formation were studied for laser milling operations on polymer laminates. It was observed that the HAZ increased whenever heat diffusion was promoted and the burnt material was accumulated on the hole surface [11]. These studies mainly dealt with the processing parameters of laser etching or drilling for a variety of polymers, concentrated primarily on the micro-holes with the depth of micrometer scale. An investigation focused on the relationship between processing parameters and the surface morphology or microstructure of the hole sidewall is still lacking, especially for laser drilling of polymers with the depth >1 mm.

In order to understand the material-removal mechanism for laser drilling of polymers, many researchers have made efforts to predict the process occurring at the laser-polymer interaction zone. The Srinivasan-Smrtic-Balu (SSB) model was formulated for excimer UV laser etching of polymers [12], which related the laser energy to the drilling depth by combining a theoretical equation of photothermal ablation with that of photochemical ablation. Also, mathematical equations were adopted to predict the quantitative depth and area of laser ablation considering a purely thermal effect, which were based on the experimental results under different laser powers and number of pulses for 1064 nm nanosecond pulsed laser drilling [13]. However, the mechanisms of mass transfer and the melt dynamics during the drilling process have not been well understood, as laser ablation is subject to the specific laser wavelength and the materials used. That is, the analysis and discussion about material-removal mechanism involving photothermal or photochemical reactions have been rarely addressed.

Hence, it is crucial to conduct a more comprehensive investigation focused on the surface morphology and microstructure of the ablation zone and make a deep understanding of laser-polymer interaction, in order to further improve the machining quality. A large number of experiments on single-pulse laser drilling of PEEK had been conducted in our previous work [14]. Hole morphology and keyhole evolution during drilling process had already been discussed. In this paper, the surface quality and microstructure of the hole sidewall were characterized by studying the following aspects: (i) surface morphology of the hole sidewall under different single-pulse energy using laser scanning confocal microscope and scanning electron microscope. (ii) microstructure of the hole sidewall using energy dispersive spectroscopy, X-ray diffraction, and Raman spectroscopy. (iii) HAZ thickness of the hole sidewall calculated by a viscous flow model. In addition, in-situ observation and analytical calculation were carried out to investigate the material-removal mechanism of the laser-polymer interaction.

2. Experimental setup and material characterization

2.1. Machining experiments

Laser drilling experiments were carried out with a quasi-continuous wave Nd: YAG fiber laser with an output fiber core of 14 μm and wavelength of 1070 nm. It is with the advantages of stable Gaussian beam distribution, rapid response time and constant peak power. Fig. 1 shows the experimental setup of laser drilling. It is primarily made up of laser system, high-precision three-axis positioning and motion platform, coaxial argon gas blowing system, real-time charge-coupled device (CCD) monitoring system, high-speed camera observation system, waveform generator and self-developed clamps with a “sandwich” structure.

In the present study, laser output was modulated as a rectangular pulse wave by the waveform generator. The nozzle assembly features a co-axial nozzle of 1.0 mm exit diameter, with a 150 mm focusing lens and a 100 mm collimating lens. The optical assembly can be adjusted to maintain the focal position of the laser beam on the centerline at the top of the work-piece surface, through vertical motion of the three-axis positioning and motion platform. The laser processing parameters can be found in Table 1. In order to characterize drilling quality relative to the specific parameters, the single-factor experiments were conducted. The effects of single-pulse energy on surface morphology and microstructure of the hole sidewall were investigated.

2.2. Material characterization

PEEK5600G workpieces of 100 mm × 50 mm × 3 mm were used for the experiments of laser drilling. Main thermal and physical parameters are shown in Table 2. The section of PEEK sample was polished with sandpapers for better surface roughness. Ultrasonic cleaning in alcohol was carried out for all the samples for 30 min before machining. Ra and Rq were nearly 0.51 μm and 1.03 μm, respectively, measured by the laser scanning confocal microscope (LSCM).

Two identical PEEK samples were pressed together on the self-developed clamps, which were fixed by a sandwich structure consisting of two metal plates, as shown in the small image embedded in the lower right corner of Fig. 1. The laser beam was focused on the junction line of two PEEK samples with the aid of coaxial CCD and Dino-lite digital microscope. Three holes were drilled for each set of processing parameter in order to achieve high accuracy of the results. After drilling, the two PEEK samples were split and a half-hole appeared on each one. Thus, the sectional morphology of the hole can be obtained right after the experiment. This method provides an instantaneous geometric shape, surface state of the hole sidewall without additional post-processing, as schematically shown in Fig. 2.

In order to better observe the physical process of laser drilling, an in-situ observation was conducted by the high-speed camera during drilling process. One PEEK sample was sandwiched by two transparent glass plates, which were held in place by two metal plates on the clamps. With the aid of Dino-lite digital microscope and CCD, the laser beam was focused on the junction line between the glass sheet and the PEEK sample. And the high-speed camera was focused on a side view of the PEEK that was parallel to the direction of the incident laser beam. Its resolution, recording rate, and shutter speed were set from 144 × 230 pixels to 128 × 50 pixels, 20,000 fps to 100,000 fps, 1/500,000 s to 1/100,000 s, respectively.

Three-dimensional LSCM was used to investigate and characterize the surface morphology and HAZ thickness of the hole sidewall. Also, the whole sectional morphology of the hole sidewall was analyzed in detail by field emission scanning electron microscope (SEM). The samples were sputter-coated with gold in advance. Energy dispersive spectroscopy (EDS) was used to determine the contents of C and O at an acceleration voltage of 8 kV. The X-ray diffraction analysis (XRD) was performed to provide information on the crystallinity and structure of

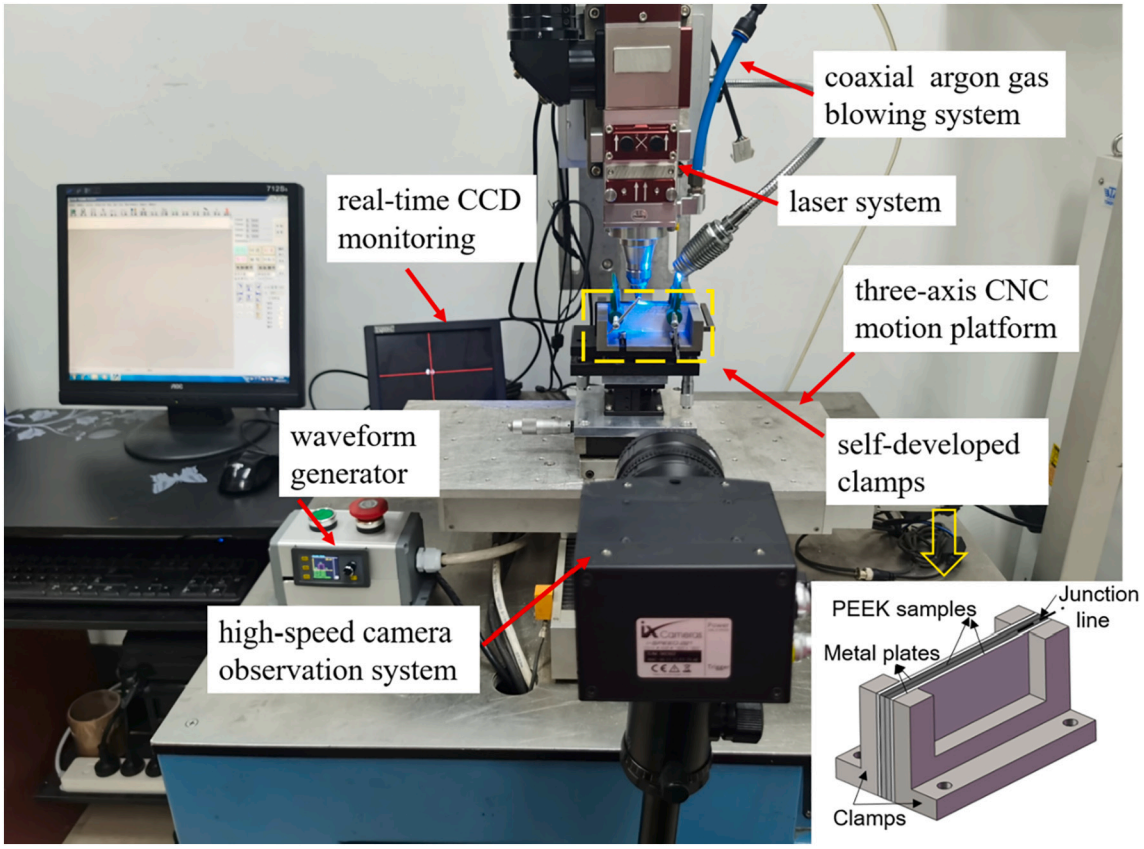

Fig. 1. Experimental equipment for laser drilling of PEEK.

Table 1
Processing parameters used in laser drilling of PEEK experiments.

Parameters	Peak power (W)	Pulse width (ms)	Defocus distance (mm)	Beam quality M^2	Rayleigh length (μm)	Assisted gas pressure (MPa)	Waist diameter (μm)
Value	100–1000	0.05–20	0	1.05	300	0.4	21

Table 2
Thermal and physical parameters of PEEK5600G [15,16].

Thermal and physical parameters	Value
Density	1.3×10^3 kg/m^3
Specific heat capacity	2200 J/(kg·K)
Thermal diffusivity	1×10^{-4} m^2/s
Thermal conductivity	0.29 W/(m·K)
Coefficient of the thermal expansion	4.7×10^{-5} /K
Glassy transition temperature (T_g)	416 K
Melting point	668 K
Vaporization temperature	668–773 K
Kinematic viscosity of molten phase	0.23–0.26 m^2/s

the hole sidewall employing the 2θ values from 10° to 60° and scanning rate of 2°/min. Raman spectra were obtained by a Raman spectrometer emitting at a laser wavelength of 514 nm with a power of 2.5 mW for chemical structural analysis.

3. Results and discussion

For laser drilling or ablation of polymers, the material is normally removed as the melt flow, vaporization, droplet or spatter [11]. During laser drilling, the heat from the laser irradiation is transferred to the adjacent substrate, and subsequent melting and re-cooling of the material will result in changes in the area surrounding the hole sidewall. Because the temperature of molten polymer drops down quickly, some irregular microscale structures, incomplete melt expulsion and fragments often remain on the surface of the hole sidewall, consequently causing inhomogeneous microstructures and decreasing the processing quality [17]. Even the chemical composition may change after the laser irradiation.

3.1. Surface morphology of the hole sidewall

For laser processing of polymers under different energy irradiation, the HAZ seems to be unavoidable, which is considered a major obstacle to its wide industrial applications [15]. Therefore, the surface morphology of the hole sidewall needs to be analyzed as the energy changes. In this study, the cross-sections of micro-holes were observed using above experimental device by LSCM. The entire hole sidewall could be divided into three parts. They were expanded zone at the entrance, linear zone in the middle and U-shaped zone at the bottom, respectively, as shown in Fig. 3(a). Fig. 3(b) shows a scheme with a typical section of laser drilling specimen and the quantification of HAZ dimension. Three positions were taken on each side of the three parts of the hole sidewall, so that the average value of the six positions on both sides was taken as the HAZ thickness to reduce the experimental error.

The sectional morphology of the hole sidewall under different single-pulse energy is shown in Fig. 4. The left image represents the whole sectional morphology of the hole sidewall. The right images are the corresponding enlargement of selected area in three parts of the sidewall

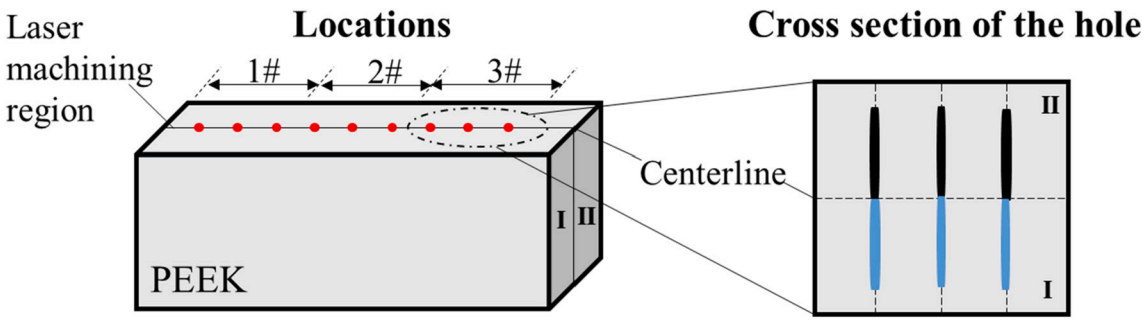

Fig. 2. Schematic of laser drilling samples of PEEK.

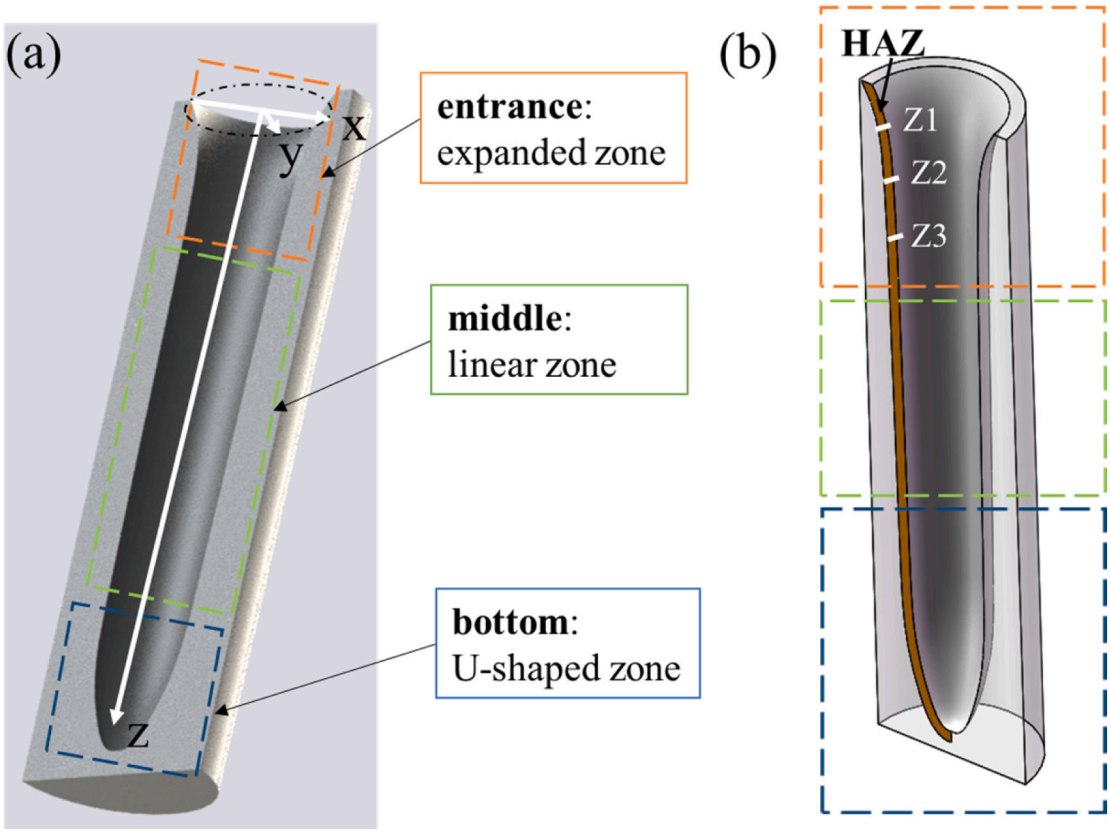

Fig. 3. Schematic diagram of the whole sectional morphology of the hole sidewall. (a) quasi-three-dimensional hole and its three parts, (b) cross section of the hole sidewall showing HAZ dimension.

from left images. There was significant change of the sectional morphology under different single-pulse energy, varying from 0.1 J to 2 J. Under the low single-pulse energy (0.1 J, 0.5 J, and 1 J), there was obvious melting phenomenon, accompanying extended HAZ at entrance of the hole sidewall. A large area of HAZ was shown at three parts of the hole sidewall, with poor surface quality. There was a fusion taper in the expanded zone at the entrance. It could be noticed that the HAZ at the entrance was the most obvious compared with the other two parts. While the linear zone in the middle was relatively homogeneous, with nearly the same HAZ thickness. For the bottom sidewall, there was obvious HAZ. Even large quantities of debris and fragments were observed in and around three zones when the single-pulse energy was 0.1 J, showing a strong adhesion. By contrast, under higher single-pulse energy (1.2 J, 1.5 J, 2 J), three zones of the sidewall looked much smoother. It can be noticed that when the single-pulse energy was over 1 J, the HAZ on the sidewall gradually decreased and nearly disappeared at the entrance and middle zones. There were only a few debris and fragments remaining on the ablated area, especially at the bottom of the hole.

Table 3 shows the HAZ thickness at entrance, middle, and bottom of the hole sidewall, which was irradiated under different single-pulse energy. The results indicated that under the low energy (0.1 J, 0.5 J, 1 J), the HAZ thickness in the middle decreased gradually from 28.2 μm to 17.5 μm. When the single-pulse energy was high enough (>1 J), it decreased slowly from 17.5 μm to 15.6 μm and almost kept constant at 1.5 J and 2 J. For the HAZ thickness of the bottom, it showed little dependence on the increment of single-pulse energy. The HAZ thickness was between 24 μm and 30 μm, presenting a small fluctuation with the increase of single-pulse energy. For the HAZ thickness at the entrance of the hole, it showed an overall decrease tendency when the single-pulse energy increased to 2 J. Under low single-pulse energy, the incident laser energy was subsequently converted into thermal energy. The material would be in a molten state. After melting, vaporization and keyhole formation occurred at high temperature. At this stage, thermal

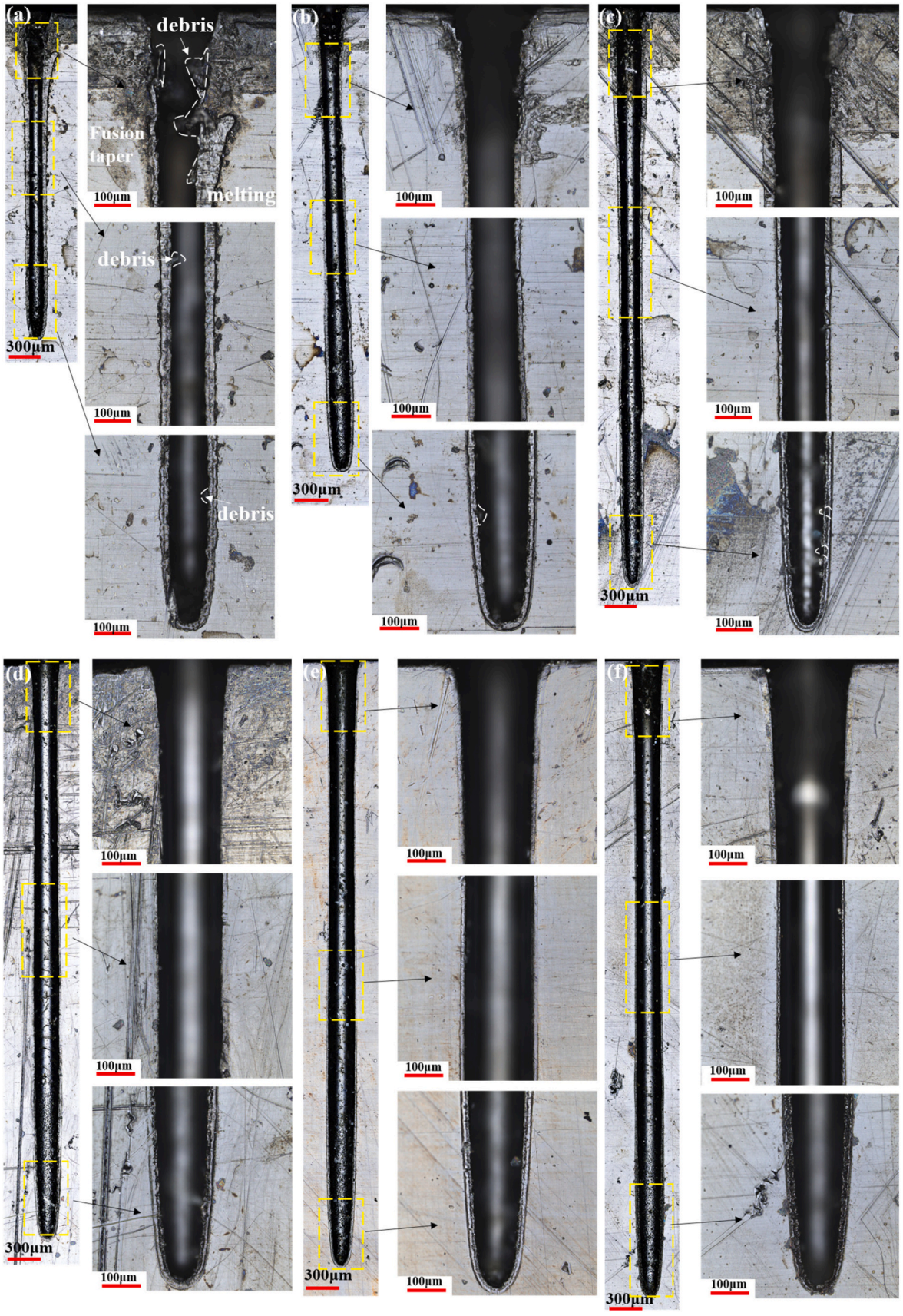

Fig. 4. Sectional morphology of the hole sidewall under different single-pulse energy: (a) 0.1 J, (b) 0.5 J, (c) 1 J, (d) 1.2 J, (e) 1.5 J, (f) 2 J.

Table 3
HAZ thickness at entrance, middle and bottom under different single-pulse energy.

Single-pulse energy (J)	HAZ thickness		
	Entrance (μm)	Middle (μm)	Bottom (μm)
0.1	43.6	28.2	28.1
0.5	28.0	23.8	26.1
1	31.9	17.5	28.4
1.2	21.4	17.1	25.8
1.5	20.3	15.8	24.6
2	22.9	15.6	30.4

effect was dominant in three zones accompanied by large HAZ thickness. With the increase of single-pulse energy, it was considered to be direct decomposition of the material at sufficiently high energy densities. Therefore, the HAZ thickness gradually decreased for the entrance and middle zones of the hole sidewall. Considering the variation of HAZ thickness at the bottom, the change of single-pulse energy had little effect on it. This was probably because the multiple reflections from the hole sidewalls would cause a lot of energy loss. And a small portion of the remaining energy contributed to the melting of the material.

Fig. 5 shows the variation of surface roughness profile with single-pulse energy increasing. Table 4 shows the values of Ra and Rq of the hole sidewall. Ra and Rq are the arithmetical mean roughness and root-mean-square roughness, respectively, which are used to assess the surface topography and heterogeneity of the hole sidewall. From Fig. 5 and Table 4, it is pertinent to note that the surface roughness Ra and Rq decreased gradually with the increase of irradiation energy. There was obvious fluctuation at the bottom of the hole sidewall when the energy was <1 J. This might be due to some cluster and fragments adhering to the inner wall after solidification, resulting in poor finish. But when the energy was over 1 J, Ra and Rq were significantly lower than that at 0.1 J and 0.5 J. The surface roughness Ra was 5.5 μm at the energy of 2 J, which was one third of Ra at the energy of 0.1 J. Considering the least adhesion and clean sidewall, the roughness profile varied uniformly from the hole entrance to bottom under high energy.

According to above results, the surface morphology of the hole sidewall varied greatly with the increment of singe-pulse energy. These phenomena could be explained from the consumption of laser energy and its density distribution both spatially and temporally. For the long pulse laser drilling, the shielding effects of the plasma and vapor cluster on the incident laser radiation occurred instantaneously, which caused the nonlinear energy absorption of material and energy loss. Under the low energy, it was accumulated on the irradiated surface from the beginning, and penetrated as the drilling depth increased. There was intense laser-induced plasma, resulting in the ejection from the region near the hole entrance and generation of HAZ. Recoil pressure caused by vapor cluster was relatively small, which further affected the ablation depth. This phenomenon was also observed in laser drilling of other polymers [18]. At the same time, a “sputter cone” geometry was formed caused by the plasma, which could be the reason for the HAZ expansion at the entrance of the hole sidewall. During deep micro-holes drilling, in the middle of the hole sidewall, the propagation and refraction of the laser beam were stable. Incident laser beam energy was deposited on the middle sidewall randomly and uniformly, causing the material to melt and re-cool with uniform surface morphology like small HAZ thickness and surface roughness.

Under high radiation energy, the recoil pressure increased with the increase of energy density, causing part of material to be removed directly in the form of decomposition without melting. Therefore, the HAZ was less obvious and its thickness was smaller, resulting in a smoother sidewall. At the bottom of the hole, the irradiation energy decayed below the ablation threshold. Considering the spatial Gaussian distribution of laser beam, the ablation front under high energy density could induce a U-shaped fusion. Unavoidably, there was still some HAZ accompanying the occurrence of melting phenomenon and the formation of debris.

3.2. Microstructure of the hole sidewall

During laser drilling of polymers, the microstructure of the laser ablation zone may change [17]. Therefore, the observation of the microstructure is helpful to understand the material-removal mechanism of polymers. In order to further obtain and analyze the microstructure of the micro-holes, the sectional topography of the hole sidewall was represented by a series of quasi-three-dimensional images by LSCM, as shown in Fig. 6.

In Fig. 6, the left image represents the whole sectional morphology of the hole sidewall. The right images are the corresponding enlargement of three selected areas from the entrance, middle and bottom of the sidewall from left images. It can be clearly seen that when the single-pulse energy varied from 0.1 J to 2 J, there was different adhesion phenomenon on the inner wall of three parts. A large number of fragments and cluster matter were observed adhering at the entrance of the hole under low energy (0.1 J, 0.5 J, and 1 J). As the energy increased, the hole sidewall at the entrance became cleaner, with little cluster matter or debris remaining on the surface. For the middle of the hole, the adhesion on the sidewall was the least compared with two other parts. This indicated that the best quality could be obtained in the middle of the hole sidewall during drilling process. Only at 0.1 J, some cluster appeared obviously in the middle of the sidewall. However, for the bottom of the sidewall, there was no significant difference although the energy increased from 0.1 J to 2 J. It could be explained that under low single-pulse energy, the material was in molten state and a small portion was removed by evaporation or ejection. The melt was deposited on the hole sidewall in the form of fragments and cluster, especially at the entrance of the hole. This was because that the recoil pressure was too small to make the molten materials to flow or be ejected out completely. Thus the photothermal effect was obvious under low energy.

The formation of the fragments and cluster was believed to result from lack of laser energy accumulation. During the drilling process, the material was removed in the form of sputtering, which usually consisted of small-scale clusters and fragments. Accordingly, large size of fragments formed due to the aggregation of clusters. They were produced when the laser irradiation energy was greatly over the ablation threshold. To demonstrate the effect of single-pulse energy on the ejection generation, the ejection of cluster and fragments were captured by the high-speed camera at the laser energy of 0.5 J, 1 J, and 1.5 J, as shown in Fig. 7.

It can be noticed that there was more ejection shown above the hole entrance with the single-pulse energy increasing. The recoil pressure induced by evaporation was high under high laser energy. On the irradiated zone, the recoil pressure contributed to the material removal, expelling the molten material out of sidewalls or pushing the incoherent material far away from the groove [19]. Thus the formation of liquefied state and decomposition of material could be affected by the recoil pressure. When drilling under low laser energy (<1 J), the energy density was very small. Recoil pressure was not high enough to make the debris ejected as completely as possible. Therefore, there were more fragments adhering and accumulating on the hole sidewall, resulting in more absorption and reflection of laser energy and affecting further machining. For the high processing energy (>1 J), it was over the ablation threshold greatly and the high recoil pressure could increase ablation depth and improve the efficiency of the laser drilling [20]. The majority of these debris and particles would be ejected out of the micro-holes. However, at relatively high laser energy, the high aspect-ratio, which is defined as the ratio of hole depth to diameter, could hinder the ejection of debris. The debris within the entrance of side walls could be easily spread out, while the ones at bottom were much more difficult to be ejected, leading to residual adhesion on the hole sidewall.

The microstructure of three parts was studied by SEM at the low

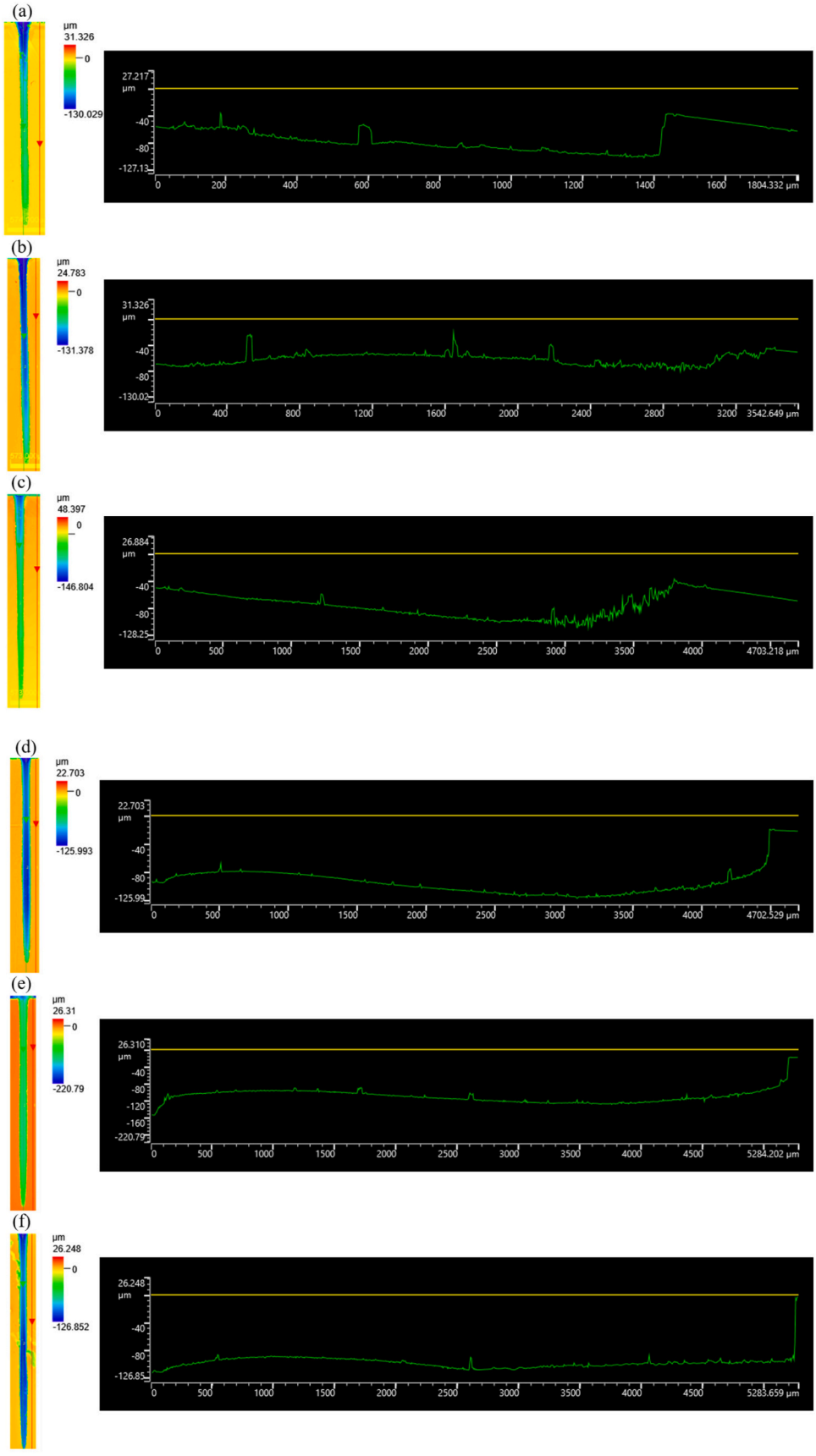

Fig. 5. Surface roughness profile under different single-pulse energy: (a) 0.1 J, (b) 0.5 J, (c) 1 J, (d) 1.2 J, (e) 1.5 J, (f) 2 J.

Table 4
Surface roughness Ra and Rq of the hole sidewall under different single-pulse energy.

Single-pulse energy (J)	Surface roughness	
	Ra (μm)	Rq (μm)
0.1	17.7	24.5
0.5	15.9	19.1
1	14.4	20.3
1.2	12.1	19.5
1.5	8.9	13.2
2	5.5	9.8

energy (0.5 J) and high energy (1.5 J), as shown in Fig. 8. The second column is the enlarged images corresponding to three parts. At the low energy, there was significant thermal ablation on three parts of the hole sidewall, showing a poor surface quality. It can be noticed that large area of HAZ occurred with many expanding bubbles and micro-pores, especially in the middle and bottom. While at the high energy irradiation, there was almost no HAZ shown on the hole sidewall. The hole surface at the entrance and middle was smooth. But at the bottom, the hole sidewall was still accompanied by diffuse micro-pores. This indicated that for the low energy irradiation, melting, micro-pores or bubbles were observed as the result of laser heating. Thermal effect would lead to serious porosity. And the hydrodynamic motion of the molten material could be correlated to the microstructure of ablation zones due to thermal gradients and surface tension gradients. For high energy irradiation, there might be direct decomposition in addition to heating and melting at high temperature for a small fraction of materials. Therefore, there was no obvious HAZ shown at the entrance and middle of the hole sidewall.

Besides, the C and O contents of three parts of the hole sidewall were measured by face scanning of EDS, as shown in the third column of Fig. 8. For the same part, the C content at the entrance under high energy was larger than that at the low energy. For three parts of the hole sidewall, there was no significant difference in C and O contents both under low energy and high energy. The C content at the entrance was slightly higher than that for the other two parts. For the laser ablation of other polymer like polyimide [21], the results showed that the C content increased and O content decreased in the ablated area, which could be explained as being induced by photothermal or photochemical decomposition of the polymer.

Fig. 9 shows the XRD images of the hole sidewall radiated at the low energy (0.1 J, 0.5 J) and high energy (1.5 J, 2 J). Under low energy (<1 J), it can be noticed that the different diffraction peaks were detected at 2θ equal to 18.99°, 20.98°, 22.96°, and 28.97°, corresponding to (110), (113), (200) and (213) crystal face indices. They were consistent with the diffraction peaks of PEEK matrix before laser drilling. The red circle represented diffraction peaks of the original PEEK matrix in Fig. 9. This indicated that the chemical structure of the hole sidewall didn't change in the case of low-energy ablation. Under high energy (>1 J), the new diffraction peaks appeared at 2θ equal to 18.86°, 20.84°, and 29.06°, corresponding to (110), (112), and (212) crystal face indices. These diffraction peaks corresponded to the new structure associated with the ablation region. The structural unit was shown by the blue triangle in Fig. 9. In addition, it can be found that the intensity of the diffraction peaks after irradiation was higher than that of the matrix. And the diffraction peaks of three parts of the hole sidewall were almost coincident when the single-pulse energy was over 0.1 J. Only at 0.1 J, the diffraction peaks at the entrance showed the difference from that for the middle and bottom. It could be demonstrated that under high laser energy, the appearance of new diffraction peaks might be due to photochemical effects induced by the decomposition of the material and the breaking of some chemical bonds.

Crystallinity of semi-crystalline polymers affects their degradation and physical properties [22]. In order to compare the change of crystallinity before and after laser irradiation, crystallinity of three parts of the hole sidewall was gained based on their XRD patterns, as shown in Table 5. The crystallinity was determined as the area of crystalline peaks divided by the sum of the areas of crystalline and amorphous peaks. According to Table 5, it can be proved that the crystallinity of the hole sidewall decreased after laser energy irradiation and some semi-crystalline structure had been transformed into amorphous structure. This is in good agreement with the studies by others that the laser irradiation could convert solid thermoplastic polymers into the amorphous structure with three-dimensional porous [23]. It can also be seen under different single-pulse energy from Table 5, the crystallinity of the hole sidewall did not change much as the energy increased.

Raman spectroscopy is used to provide chemical and structural characterizations of the hole sidewall. It is allowed to get a statistical study on Raman peak parameters such as the intensity of the major peaks. Fig. 10 shows the Raman spectra of PEEK matrix and three parts of the hole sidewall after laser irradiation. Under low energy (<1 J), the identical vibrational bands between the matrix and irradiated areas could be observed, i.e.: C—H out-of-plane deformation of phenylene rings (809 cm^{-1}), C–O–C stretching vibration (1148 cm^{-1}), phenylene ring stretching (1597 cm^{-1}), carbonyl stretching (1647 cm^{-1}), and C—H in-plane stretching of phenyl rings (3069 cm^{-1}) [24]. Relative intensities of these bands of three parts were slightly higher than the matrix. It could be concluded that almost no compositional differences were observed. Thus no significant chemical changes were induced by the laser radiation under the low energy. For the high energy (>1 J), the changes in relative peak intensity were mainly identified as the out-of-plane deformation of phenylene rings, stretching vibration, phenylene ring stretching, carbonyl stretching and in-plane stretching of phenyl rings. The relative intensities of the C—H bond decreased, which was associated with chain scission at the link to the phenyl ring (809 cm^{-1}, 3069 cm^{-1}). And the relative intensities at the wavenumber of phenyl ring (1597 cm^{-1}) and C–O–C (1148 cm^{-1}) decreased, which were assumed to break up and cross-link with the surrounding polymer or the atmosphere [23]. Therefore, it is possible to identify different degradation peaks due to extensive polymer sputtering and decomposition. From Fig. 10, by comparing the intensity changes of the peaks at low energy and high energy, it could be concluded that laser ablation would cause the fracture of some chemical bonds under high energy, contributing to mass removal of the keyhole.

3.3. A model for evaluating the HAZ thickness

Knowledge of material-removal mechanism and attainable surface quality are crucial to the development of laser drilling of polymers. When the laser beam is irradiated on the surface of polymer, the material is heated. During the drilling process, the polymer would be in molten state due to the photothermal effect. After melting, vaporization, ejection and keyhole formation occur under the recoil pressure determined by the absorbed energy. And the HAZ is observed on the hole sidewall. Therefore, it is important to understand the physical process of polymer ablation and evaluate processing quality such as HAZ thickness. An analytical model was developed to calculate the HAZ thickness by solving the momentum equation for viscous melt flow after some simplifications. Fig. 11 shows the 2-D axisymmetric cylindrical coordinate system used for formulating the physical process of laser drilling.

In Fig. 11, r denotes the radical direction and z originates at the free surface of the molten zone and points to the molten-solidified interface. The material is removed along the z-axis, which is penetration direction of the laser beam. h represents the HAZ thickness of the hole sidewall. The general form of the governing equation for the conservation of momentum can be expressed by Eq. (1). For further simplification of the physical equation, the following assumptions were made:

1. The molten flow of material was assumed to be steady, viscous and incompressible laminar flow.

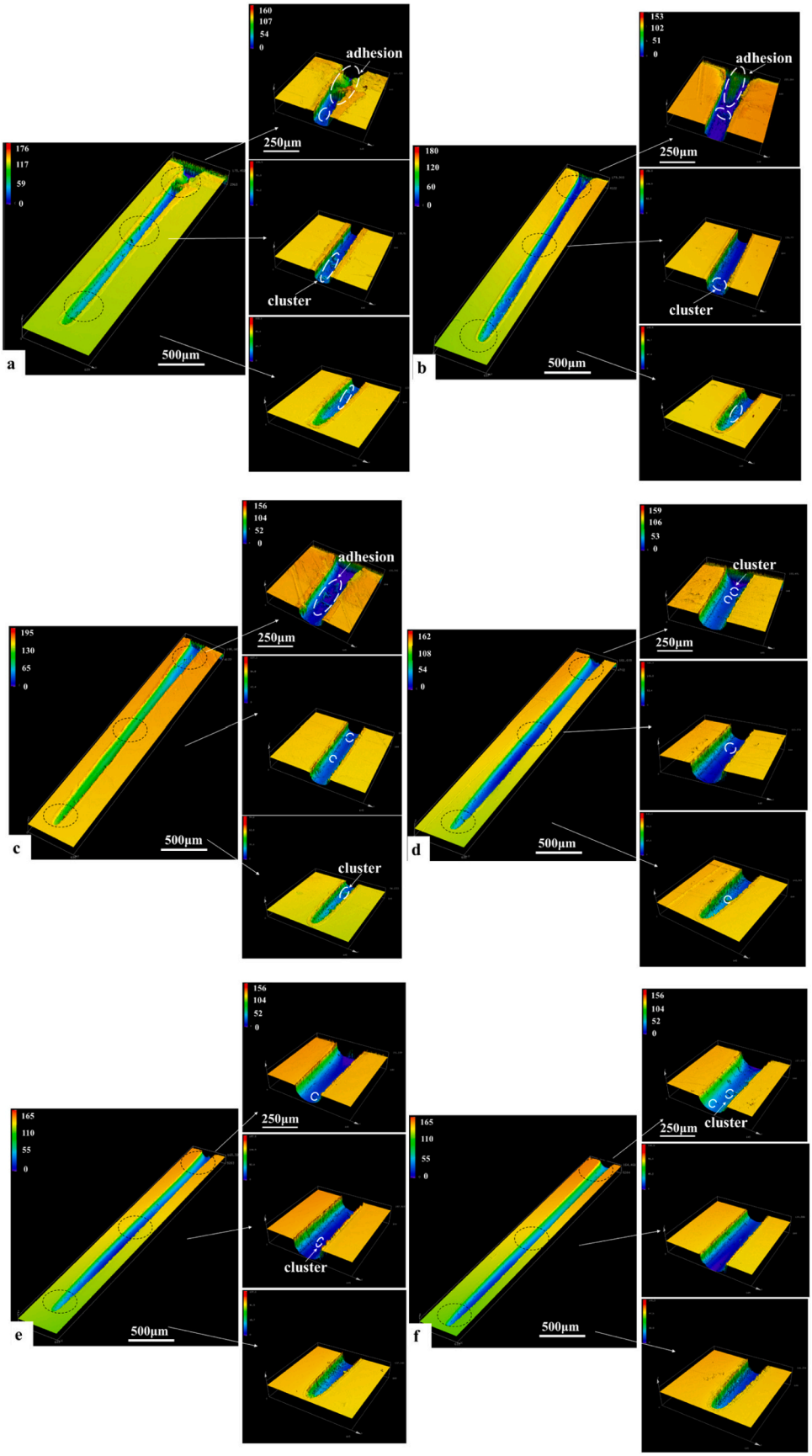

Fig. 6. Quasi-three-dimensional sectional topography of the hole sidewall by LSCM under different single-pulse energy: (a) 0.1 J, (b) 0.5 J, (c) 1 J, (d) 1.2 J, (e) 1.5 J, (f) 2 J.

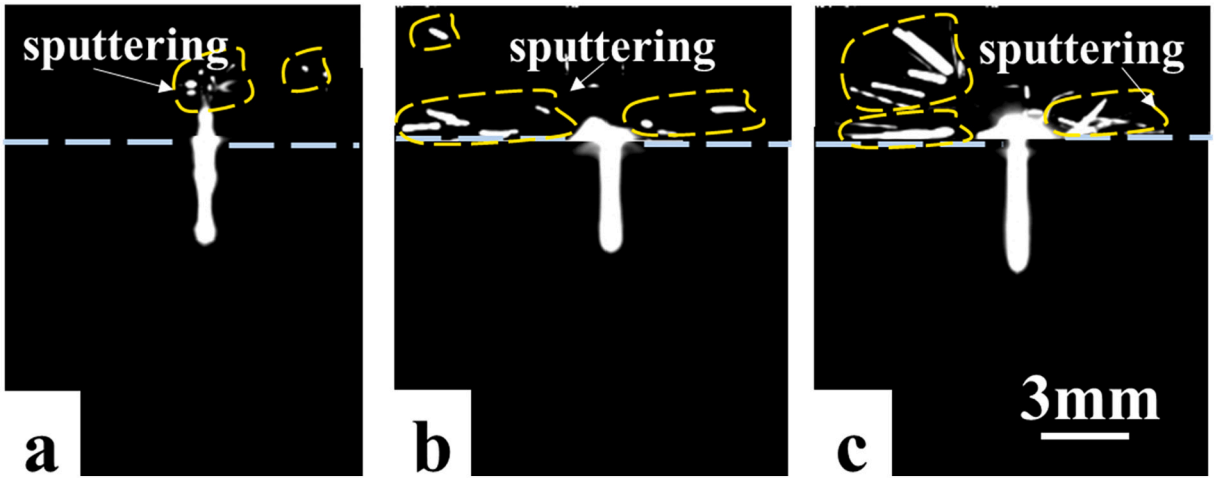

Fig. 7. In-situ observation of drilling process by the high-speed camera under different single-pulse energy: (a) 0.5 J, (b) 1 J, (c) 1.5 J.

2. The generalized Newtonian fluid was used when the temperature was above the glassy transition temperature.
3. The physical properties of the melt flow were constant, like the density and the viscosity.
4. The lateral velocity was much larger than the vertical component in the melt layer, which enabled to simplify the governing equations considerably.
5. The gravitational force was ignored.

Based on the above assumptions, the governing equation of viscous molten flow could be written as Eq. (2).

$$\rho\frac{\partial u}{\partial t}+\rho(\vec{u}\cdot\nabla)\vec{u}=\nabla\cdot\left[-PI+\mu\left(\nabla\vec{u}+(\nabla\vec{u})^{\mathrm{T}}\right)\right]+\rho\vec{g}+\vec{F}_{vol} \tag{1}$$

$$u_r\frac{\partial u_r}{\partial r}+u_z\frac{\partial u_r}{\partial z}=\nu\left(\frac{\partial^2 u_r}{\partial z^2}+\frac{1}{r}\frac{\partial u_r}{\partial r}-\frac{u_r}{r^2}\right)-\frac{1}{\rho}\frac{\partial P}{\partial r} \tag{2}$$

where u, u_r and u_z are the generalized, radical and vertical velocities (along r-axis and z-axis), respectively. ρ is the density of the melt. μ, I, g and F_{vol} are the dynamic viscosity, identity matrix, gravity acceleration and body force, respectively. ν and P represent the kinematic viscosity and the recoil pressure induced by the ablation process. Because the viscosity of polymer after melting is larger than the general fluid, the Reynolds number which represents the ratio of the inertial force to the viscous force is much smaller. Further, considering the steady-state phase, Eq. (2) has the form of Eq. (3) after neglecting these terms:

$$\frac{\partial^2 u_r}{\partial z^2}=\frac{\partial P}{\nu\rho\partial r} \tag{3}$$

For $z=0$, it is the position of the free surface; For $z=h$, it is the position of the molten-solidified interface. During the drilling process, the pressure gradient of ablation is induced dominantly by the high-temperature ejection of fragments, vaporization or sublimation (see in Fig. 11) [25]. It was established as Eq. (4) [26].

$$t=\frac{h^2}{\nu} \tag{4}$$

where t is the time of stationary viscous flow, which is induced by the gradient of ablation plume pressure. Correspondingly, the boundary conditions of the free surface are as follows:

$$\frac{\partial u_r}{\partial r}=0;(z=0) \tag{5}$$

$$u_r=0;(z=h) \tag{6}$$

Combining the above equations, Eq. (3) was integrated and the solution of the velocity distribution $u_r(z)$ was given by Eq. (7). An average velocity $\hat{u}_r(r, z)$ across melting depth was calculated by Eq. (8).

$$u_r(r,z)=\frac{1}{2\nu\rho}\cdot\frac{\partial P}{\partial r}\left(z^2-h^2\right) \tag{7}$$

$$\hat{u}_r(r,z)=-\frac{h^2}{3\rho\nu}\cdot\frac{\partial P}{\partial r} \tag{8}$$

In Fig. 11, for the entrance of the hole, the pressure is close to the ambient pressure. And for the transient molten flow of polymer surface, P could be written as Eq. (9) [19].

$$P=\frac{CF}{t_e} \tag{9}$$

where C is the mechanical coupling coefficient, F represents the energy density of laser radiation, t_e is the characteristic duration of pressure effect. C could be calculated according to Eq. (10) (see details in [27]):

$$C=\sqrt{\frac{2\rho L(F')}{F}} \tag{10}$$

where $L(F')$ is the drilling depth, which is dependent on radiation energy. Eq. (11) shows the relationship between the drilling depth and radiation energy. It was obtained by fitting a set of experimental data, which were represented in reference [12] in detail.

$$L(F')=1.31*ln(F')+4.32 \tag{11}$$

And it could be obtained:

$$\frac{\partial P}{\partial r}=\frac{0-P}{\Gamma/2}=-\frac{2P}{\Gamma} \tag{12}$$

where Γ is the effective range of Gaussian laser radiation. Therefore, the HAZ thickness h could be calculated by Eq. (13).

$$h=\hat{u}_r(z)\times t_e \tag{13}$$

Taking Eqs. (9)–(12) into Eq. (13), h was given by Eq. (14).

$$h=\frac{3\nu\sqrt{\rho}}{2\sqrt{2}}\cdot\frac{\Gamma}{\sqrt{FL(F')}}=A_1\cdot A_2 \tag{14}$$

From Eq. (14), it could be concluded that the HAZ thickness h depended on two parts, which could be represented by A_1 and A_2. For one thing, it was determined by A_1, which was related to the material properties like the density and viscosity of molten flow; For another, it was also influenced by A_2, representing the energy of laser radiation. For

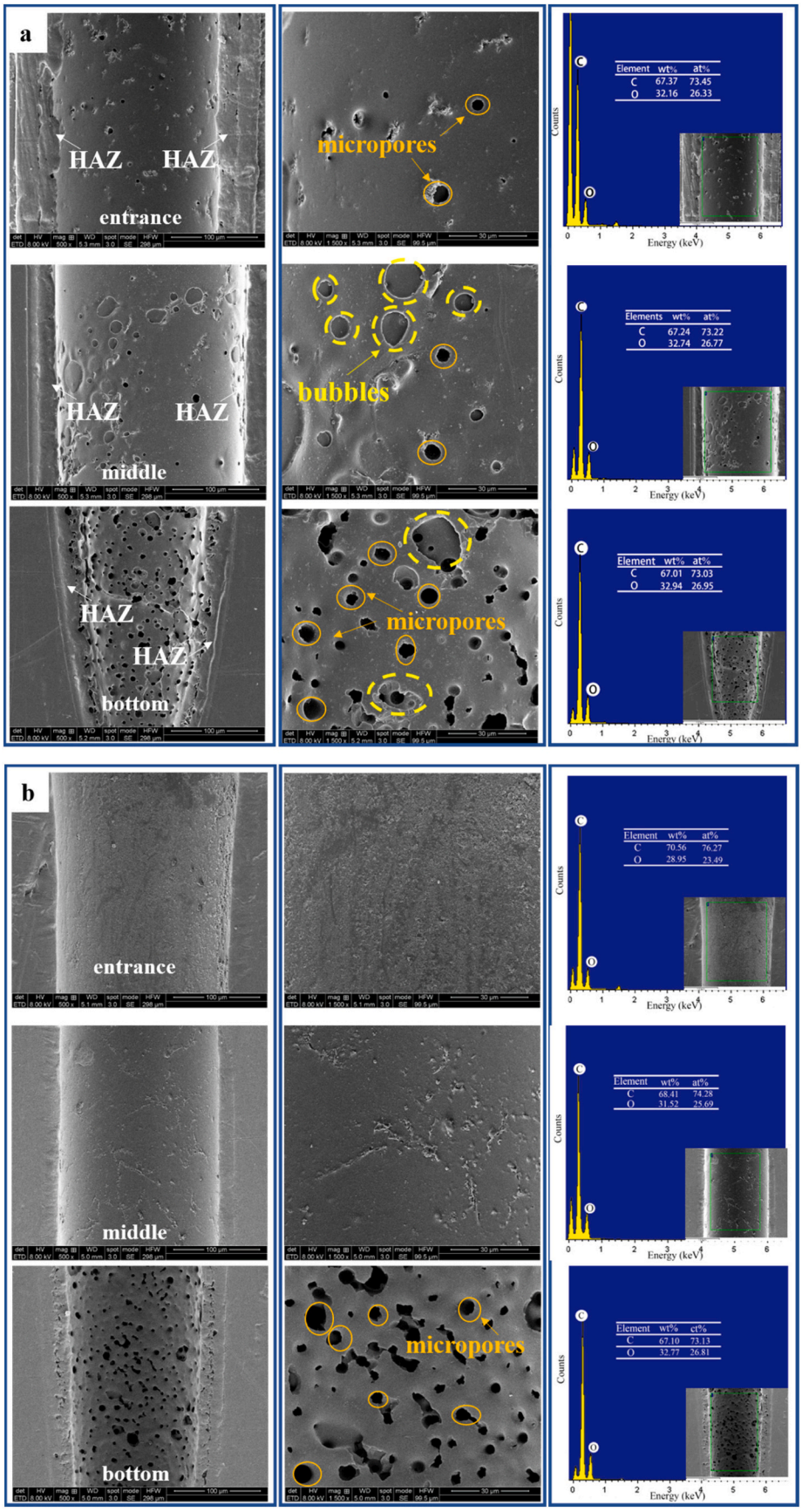

Fig. 8. SEM micrographs of three parts of the hole sidewall under different single-pulse energy: (a) 0.5 J, (b) 1.5 J.

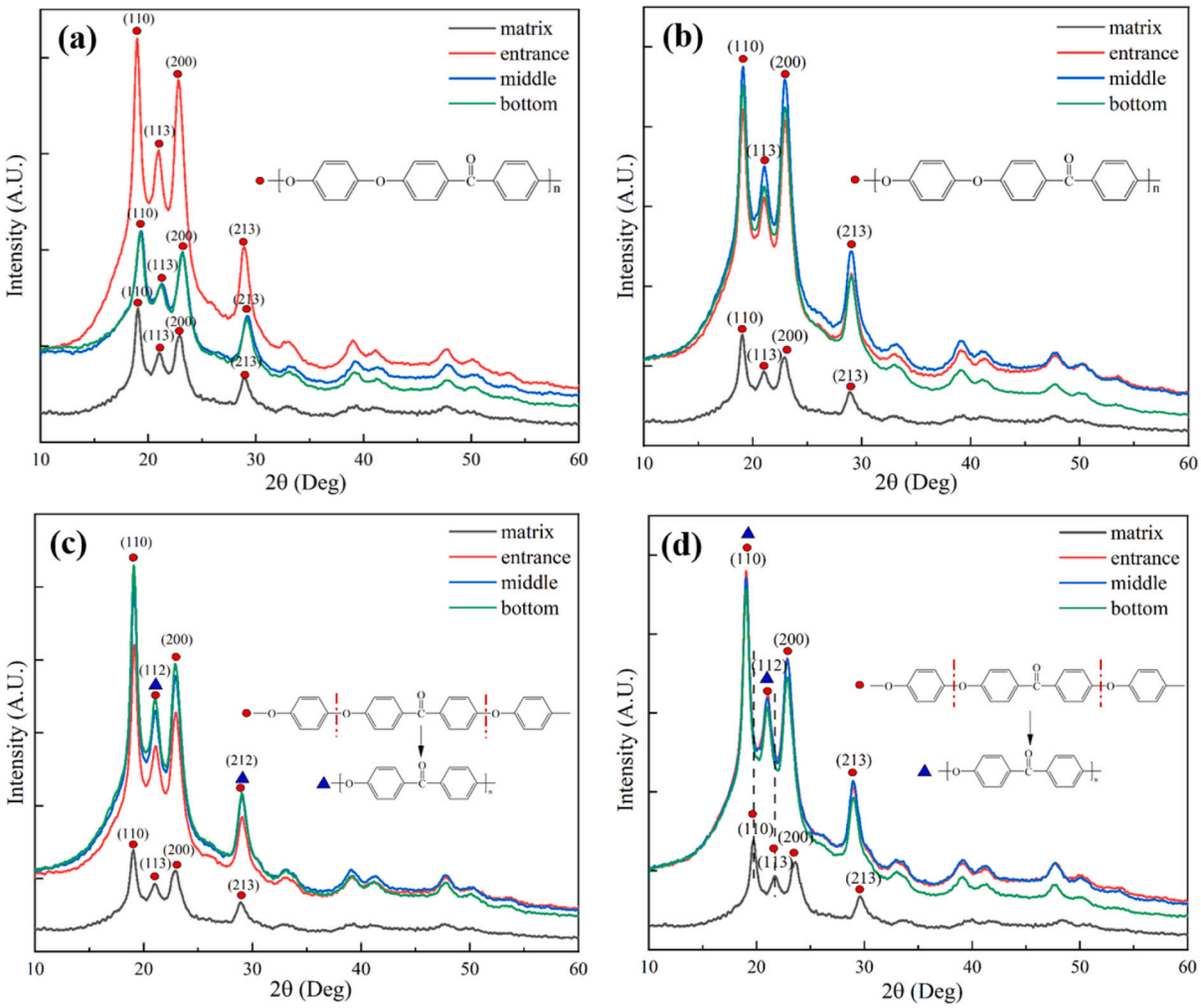

Fig. 9. XRD images of three parts of the hole sidewall under different single-pulse energy. (a) 0.1 J, (b) 0.5 J, (c) 1.5 J, (d) 2 J.

Table 5
Crystallinity of the hole sidewall before and after laser drilling under different energy.

	Matrix	0.1 J	0.5 J	1 J	1.2 J	1.5 J	2 J
Crystallinity	35.63 %	24.14 %	25.21 %	26.47 %	24.13 %	20.57 %	24.24 %

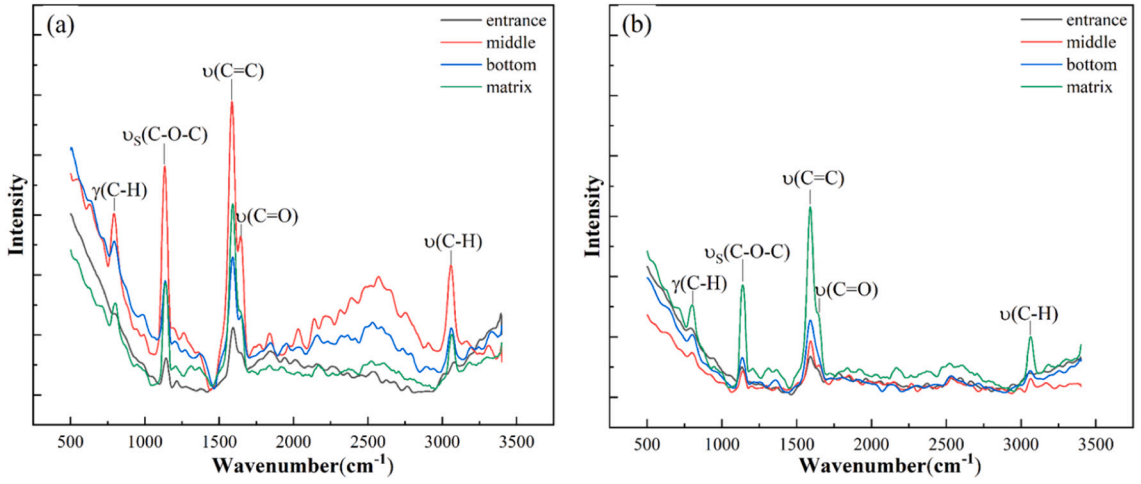

Fig. 10. Raman spectra of three parts of the hole sidewall under different single-pulse energy. (a) 0.5 J, (b) 1.5 J.

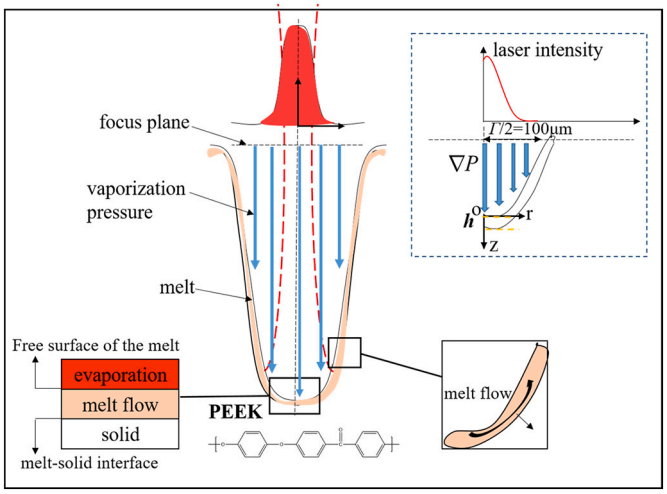

Fig. 11. Scheme of laser drilling illustrating main parameters used in the physical model.

different single-pulse energy given in the experiments, the HAZ thickness was calculated by Eq. (14). Table 6 shows the comparison between the experimental and calculated HAZ thickness in the middle of the hole sidewall. It can be noticed that there was little difference between the experimental and calculated values under different single-pulse energy. It will pave the way for better understanding of the drilling process accompanying viscous molten flow and identifying the HAZ thickness in laser ablation of polymers.

During the micro-hole machining of PEEK with single-pulse laser, it was proved that the surface morphology could be improved by an appropriate control of single-pulse laser energy. A clean hole sidewall could be obtained with little HAZ, cluster matter or debris and small surface roughness when the single-pulse energy was over 1 J. In addition, the microstructure of the hole sidewall was analyzed. Under high energy irradiation, there were direct decomposition of the material and the fracture of the chemical bonds, which was helpful to minimize HAZ thickness and improve the surface quality. This work provides a processing guide for laser drilling of PEEK and other polymers in terms of machining quality and material-removal mechanism.

4. Conclusion

In this paper, the influence of different single-pulse energy on the surface quality of the hole sidewall was demonstrated. Surface morphology and microstructure were discussed in detail. Furthermore, in order to understand the physical process of laser drilling, a physical model was proposed to calculate the HAZ thickness of the hole sidewall. Some conclusions drawn from the results are as follows:

(1) There was significant change of the sectional morphology with different single-pulse energy. The hole sidewall was divided into three parts: expanded zone at the entrance, linear zone in the middle, and U-shaped zone at the bottom. A radiation energy over 1 J was suitable, yielding an acceptable surface quality with little HAZ, uniform surface roughness and the least adhesion. By contrast, when the laser energy was <1 J, there was obvious HAZ, accompanying with many debris or fragments remaining within the ablated area. The HAZ thickness decreased with the increase of single-pulse energy, and the thickness in the middle was the smallest for different single-pulse energy.

(2) The microstructure of three parts was obviously different irradiated at low energy and high energy. There were significant expanding bubbles and holes in the middle and bottom under low energy (<1 J). The C content at the entrance under high energy (>1 J) was higher than that under low energy. The crystallinity of the hole sidewall decreased from 35 % to 25 % after laser energy irradiation but there was little change under different energy. New diffraction peaks appeared in the XRD images and the intensity of major peaks (phenyl ring (1597 cm^{-1}) and C–O–C (1148 cm^{-1})) in the Raman spectra decreased obviously under high energy. It could be concluded that it would cause direct decomposition and fracture of some chemical bonds such as the C–O–C under high energy.

(3) The HAZ thickness was calculated as a function of processing parameters and thermal properties of materials based on a viscous flow model. It was in good agreement with the experimental results under different single-pulse energy. It will pave the way for a better understanding of the physical process and material-removal mechanism involved in laser ablation of polymers.

Table 6
Comparison between the experimental and calculated HAZ thickness of the hole sidewall under different single-pulse energy.

Single-pulse energy (J)	HAZ thickness	
	Experiment (μm)	Calculation (μm)
0.1	28.2	28.9
0.5	23.8	24.6
1	17.5	17.1
1.2	17.1	16.6
1.5	15.8	14.1
2	15.6	13.1

Declaration of competing interest

The authors state that this work, or part of it, has not been published before, that it is not under consideration for publication anywhere else, and that its publication is approved by all co-authors. The authors declare that they have no conflict of interest.

Acknowledgements

This work was supported by the National Natural Science Foundation of China (No. 11672304), and Plan for Beijing Municipal Commission of Science and Technology (No. Z181100003818015).

References

[1] Villar M, Garnier C, Chabert F, Nassiet V, Samélor D, Diez JC, Sotelo A, Madre MA. In-situ infrared thermography measurements to master transmission laser welding process parameters of PEKK. Opt Lasers Eng 2018;106:94–104.
[2] Rawal S, Sidpara AM, Paul J. A review on micro machining of polymer composites. J Manuf Process 2022;77:87–113.
[3] Yuan B, Wang LN, Zhao R, Yang X, Yang X, Zhu XD, Liu LM, Zhang K, Song YM, Zhang XD. A biomimetically hierarchical polyetherketoneketone scaffold for osteoporotic bone repair. Sci Adv 2020;6.
[4] Liu L, Qu D, Cao H, Huang X, Song Y, Kang X. Process optimization of high machining efficiency and low surface defects for HSD milling UD-CF/PEEK with limited thermal effect. J Manuf Process 2022;76:532–47.
[5] Zheng YY, Xiong CD, Wang ZC, Li XY, Zhang LF. A combination of CO2 laser and plasma surface modification of poly(etheretherketone) to enhance osteoblast response. Appl Surf Sci 2015;344:79–88.
[6] Liu C, Zhang X, Wang G, Wang Z, Gao L. New ablation evolution behaviors in micro-hole drilling of 2.5D Cf/SiC composites with millisecond laser. Ceram Int 2021;47:29670–80.
[7] Zhang Y, He X, Yu G, Li S, Tian C, Ning W, Zhang Y. Dynamic evolution of keyhole during multi-pulse drilling with a millisecond laser on 304 stainless steel. Opt Laser Technol 2022;152:108151.
[8] Hartwig A, Hunnekuhl J, Vitr G, Dieckhoff S, Vohwinkel F, Hennemann OD. Influence of CO2 laser radiation on the surface properties of poly(ether ether ketone). J Appl Polym Sci 1997;64:1091–6.
[9] Shin BS, Oh JY, Sohn H. Theoretical and experimental investigations into laser ablation of polyimide and copper films with 355-nm nd:YVO4 laser. J Mater Process Technol 2007;187–188:260–3.
[10] Caprino G, Tagliaferri V. Maximum cutting speed in laser cutting of fiber reinforced plastics. Int J Mach Tool Manuf 1988;28:389–98.

[11] Leone C, Papa I, Tagliaferri F, Lopresto V. Investigation of CFRP laser milling using a 30W Q-switched yb:YAG fiber laser: effect of process parameters on removal mechanisms and HAZ formation. Compos A: Appl Sci Manuf 2013;55:129–42.
[12] Srinivasan V, Smrtic MA, Babu SV. Excimer laser etching of polymers. J Appl Phys 1986;59:3861–7.
[13] Ravi-Kumar S, Zhang X, Lies B, Jiang L, Qin H. An area-depth approximation model of microdrilling on high-density polyethylene soft films using pulsed laser ablation. J Micro Nano-Manuf 2019;7.
[14] Zhang Y, Yu G, Tian C, Li Z, Shao J, Li S, He X. Hole morphology and keyhole evolution during single pulse laser drilling on polyether-ether-ketone (PEEK). Materials 2022;15.
[15] Romoli L, Fischer F, Kling R. A study on UV laser drilling of PEEK reinforced with carbon fibers. Opt Lasers Eng 2012;50:449–57.
[16] Cheng SZD, Wunderlich B. Heat-capacities and entropies of liquid, high-melting-point polymers containing phenylene groups (PEEK, PC, AND PET). J Polym Sci B Polym Phys 1986;24:1755–65.
[17] Marchant AL, Snelling HV. Reciprocity in long pulse duration laser interactions with polymers. J Phys D Appl Phys 2012;45.
[18] Wesner DA, Aden M, Gottmann J, Husmann A, Kreutz EW. Material removal and chemical and structural changes induced by irradiation of polymer surfaces with KrF-excimer laser radiation. Fresen J Anal Chem 1999;365:183–7.
[19] Weisbuch F, Tokarev VN, Lazare S, Debarre D. Viscosity of transient melt layer on polymer surface under conditions of KrF laser ablation. Appl Surf Sci 2002;186:95–9.
[20] Li X, Hou WT, Han B, Xu LF, Li ZW, Nan PY, Ni XW. Investigation on the continuous wave mode and the ms pulse mode fiber laser drilling mechanisms of the carbon fiber reinforced composite. Polymers 2020;12.
[21] Yung KC, Zeng DW. Laser ablation of upilex-S polyimide: influence of laser wavelength on chemical structure and composition in both ablated area and halo. Surf Coat Technol 2001;145:186–93.
[22] Bhatla A, Yao YL. Effect of laser surface modification on the crystallinity of poly(L-lactic acid). J. Manuf. Sci. E. T. ASME 2009;131.
[23] Bayerl T, Brzeski M, Martinez-Tafalla M, Schledjewski R, Mitschang P. Thermal degradation analysis of short-time heated polymers. J Thermoplast Compos Mater 2015;28:390–414.
[24] Cordero D, Lopez-Alvarez M, Rodriguez-Valencia C, Serra J, Chiussi S, Gonzalez P. In vitro response of pre-osteoblastic cells to laser microgrooved PEEK. Biomed Mater 2013;8.
[25] Grabon W, Pawlus P, Sep J. Tribological characteristics of one-process and two-process cylinder liner honed surfaces under reciprocating sliding conditions. Tribol Int 2010;43:1882–92.
[26] Landau LD, Lifshitz EM. CHAPTER II - viscous fluids. In: Landau LD, Lifshitz EM, editors. Fluid Mechanics. Second Edition. Pergamon; 1987. p. 44–94.
[27] Weisbuch SLF, Tokarev VN, Debarre D. In: Proceedings of LASERAP'4. Vol. 1. France: Les Hauts de Marquay; 1–5 October 2001. p. 139–62.